THE JOURNAL OF PHYSICAL CHEMISTRY B

Article

pubs.acs.org/JPCB

Molecular Dynamics Simulation Study of the Early Stages of Nucleation of Iron Oxyhydroxide Nanoparticles in Aqueous Solutions

Hengzhong Zhang,*[,†] Glenn A. Waychunas,[‡] and Jillian F. Banfield[†,‡]

[†]Department of Earth and Planetary Science, University of California, Berkeley, California 94720, United States

[‡]Earth Sciences Division, Lawrence Berkeley National Laboratory, Berkeley, California 94720, United States

Supporting Information

ABSTRACT: Nucleation is a fundamental step in crystal growth. Of environmental and materials relevance are reactions that lead to nucleation of iron oxyhydroxides in aqueous solutions. These reactions are difficult to study experimentally due to their rapid kinetics. Here, we used classical molecular dynamics simulations to investigate nucleation of iron hydroxide/oxyhydroxide nanoparticles in aqueous solutions. Results show that in a solution containing ferric ions and hydroxyl groups, iron−hydroxyl molecular clusters form by merging ferric monomers, dimers, and other oligomers, driven by strong affinity of ferric ions to hydroxyls. When deprotonation reactions are not considered in the simulations, these clusters aggregate to form small iron hydroxide nanocrystals with a six-membered ring-like layered structure allomeric to gibbsite. By comparison, in a solution containing iron chloride and sodium hydroxide, the presence of chlorine drives cluster assembly along a different direction to form long molecular chains (rather than rings) composed of Fe−O octahedra linked by edge sharing. Further, in chlorine-free solutions, when deprotonation reactions are considered, the simulations predict ultimate formation of amorphous iron oxyhydroxide nanoparticles with local atomic structure similar to that of ferrihydrite nanoparticles. Overall, our simulation results reveal that nucleation of iron oxyhydroxide nanoparticles proceeds via a cluster aggregation-based nonclassical pathway.

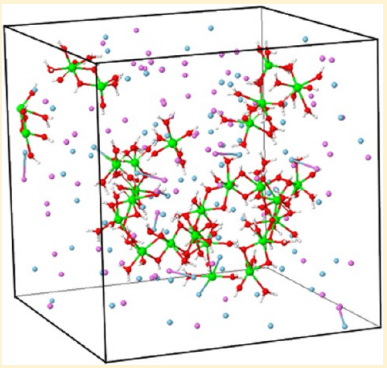

1. INTRODUCTION

Nucleation of iron oxyhydroxides is of fundamental and technical importance in many fields of science. The precipitation process has been a topic for extensive research for decades (see, e.g., refs 1−6). However, a molecular level understanding of the nucleation dynamics is lacking. For instance, the details of the reactions that transform iron monomers into larger molecular clusters and nuclei are poorly understood.

The hydration and dehydration of cations are elementary steps involved in nucleation. Various experimental techniques have been used to study the static and dynamic structures and properties of hydrated ferric cations in aqueous solutions.[7] These include X-ray/neutron/electron diffraction methods, X-ray/neutron scattering methods, X-ray absorption spectroscopy, nuclear magnetic resonance (NMR) and closely related Mössbauer spectroscopy, and infrared/Raman spectroscopies.[7] Among these, NMR can access time scales as short as nanoseconds (1 ns = 10^{-9} s) as well as longer processes.[7] With pulsed synchrotron light sources, X-ray scattering and absorption offer potential approaches with even shorter time scales for in situ study of nucleation of iron oxyhydroxides in a solution. However, these "ultrafast" methods are only now starting to be developed, and experimental work has generally probed much longer time scales. Recently, using QEXAFS and UV−vis spectroscopy, Zhu et al. found that the initial steps in monomer merging during hydrolysis of Fe^{3+} nitrate solutions involve formation of μ-oxo-bridged dimers that resist further aggregation until they rearrange into a dihydrobridged dimer.[8] However, reactions beyond dimer formation, which may happen in just tens of picoseconds (1 ps = 10^{-12} s) as suggested by the results of the present work, were too rapid to isolate using QEXAFS or other readily available techniques. In the absence of a method in which the initial steps can be tracked experimentally, we turned to a molecular simulation-based approach. Simulations are complementary to experiments as they can provide perspectives on nucleation of iron oxyhydroxides in aqueous solutions on a time scale from a few picoseconds to tens of nanoseconds.

Most prior computational work has focused on the complexation of one ferric or ferrous cation with surrounding water molecules and/or hydroxyl groups.[9−18] Efforts have been made to correctly reproduce the experimentally derived structure of the hydration shells around an iron cation using molecular dynamics (MD) simulations,[9,10,14,15,19,20] first-principle calculations,[11,18] and ab initio molecular dynamics simulations.[13,17,18,20] Density functional theory (DFT) also has been used to study the structure, energetics, and electronic properties of iron−water/hydroxyl molecular species in aqueous solutions. Martin et al.[11] studied the structures and

Received: April 21, 2015
Revised: July 27, 2015
Published: July 29, 2015

DOI: 10.1021/acs.jpcb.5b03801
J. Phys. Chem. B 2015, 119, 10630−10642

free energies of several iron monomers. Calculations by Panina et al.[21] showed that solvation resulted in higher stability of dihydroxo-bridging cations than other species. However, semiempirical quantum mechanical calculations by Lopes et al.[12] showed that ferric dimers exist in the μ-hydroxo-bridged form. In contrast, a recent experimental and DFT study[8] showed that the μ-oxo-bridged form of the ferric dimer is more stable, though it should be noted that the experimental part of the research was performed in nitrate aqueous solutions.

At present, the only affordable method for simulating iron oxyhydroxide nucleation is classical MD (CMD) due to the required time scale (e.g., tens of nanoseconds) and spatial scale (e.g., tens of nanometers). This is too large a system and too long a duration to be able to use first-principle MD simulations, due to the involvement of a huge number of electrons. Even for CMD simulations, there are no dedicated interatomic potential function sets designed specifically for iron species in both the solid phases and the aqueous solutions, which often contain cations such as Na^+ and K^+ and anions such as NO_3^-, Cl^-, and SO_4^{2-}. The reactive force field for the Fe−O−H system developed recently[22] cannot be applied to such complex solutions. Thus, studies of the early stages of nucleation of iron oxyhydroxide nanoparticles in complex aqueous solutions are very computationally challenging. Here, we combined two force field sets for iron-related compounds and tested the applicability of the contained potential functions after a necessary adjustment of some model parameters. We then used extensive MD simulations to study the dynamics of iron molecular clusters formation and cluster growth in aqueous solutions containing dissolved Fe^{3+}, Na^+, Cl^-, and OH^-. These processes lead to the formation of iron oxyhydroxide nanoparticles during neutralization reactions of ferric solutions (considering Fe^{3+} as a Lewis acid).

2. INTERACTION POTENTIAL FUNCTIONS

2.1. Choice of Interatomic Potential Functions. In CMD, atomic movements are described by Newton's second law of motion. The forces exerted on atoms are calculated using spatial gradients of the interatomic potential functions (also called force fields) that primarily consist of the pairwise interatomic interactions and additional three-body or multibody interatomic interactions.[23] Commonly, the pairwise interactions are represented by the sum of the electrostatic interactions and the van der Waals interactions. The former are described by the Coulombic law; the latter are described using various empirical equations, such as the Buckingham potential function (eq 1) and the generalized Lennard−Jones potential function (eq 2)

$$U_{ij}(r) = A\exp\left(-\frac{r}{\rho_0}\right) - \frac{C}{r^6} \tag{1}$$

$$U_{ij}(r) = \frac{E_0}{n-m}\left[m\left(\frac{r_0}{r}\right)^n - n\left(\frac{r_0}{r}\right)^m\right] \tag{2}$$

In the equations above, U_{ij} and r represent the interatomic potential and distance, respectively. A, ρ_0, C, E_0, r_0, and n and m are model parameters (constants) specific for one type of interaction pair i and j. If $n = 12$ and $m = 6$, eq 2 reduces back to the original form of the Lennard−Jones function.

De Leeuw and Cooper[24] developed a set of interatomic potential functions transferable among several solid phases of iron oxyhydroxides and iron oxides, including goethite (α-FeOOH), hematite (α-Fe_2O_3), and green rust ($Fe(OH)_2$). For studying surface hydration of some of the iron compounds, they used water molecules described by the shell model[25] of water[26] to derive the interaction potentials between the iron compounds and surface water. Molecular static calculations using this set of potential functions reproduced the crystal structures accurately, as well as some of the surface properties. Spagnoli et al.[27] proposed a set of potential functions for interfacial interactions between hematite surfaces and aqueous solutions of sodium chloride. In that study the potential functions of some species (e.g., hydroxyl and shell water) are the same as those in the de Leeuw and Cooper[24] set. This treatment offers potential compatibility of the two sets. The Spagnoli et al. set of potentials allowed MD study of the distribution and diffusion of Na^+ and Cl^- ions in the vicinity of the hematite (001) surface contacting a NaCl solution. We combined the Spagnoli et al.[27] potential set and the de Leeuw and Cooper[24] potential set for MD simulations of the iron(III) oxyhydroxide nucleation in aqueous solutions.

Iron compounds and their interactions with water have been described using the de Leeuw set;[24] NaCl solution and NaCl−iron compound interactions used the Spagnoli et al. set.[27] In MD simulations under the NPT condition, we found that the shell water model[26] did not perform well (see below). Thus, we chose a revised version (i.e., CF1 model[28,29]) of the central force model for water[30] (see Supporting Information, SI, section 2) to replace the shell water model in the two sets. For aqueous species Fe^{3+} and OH^-, we assumed that they can be described reasonably using the same potential functions as those for lattice Fe^{3+} and OH^- (i.e., those in solid phases of FeOOH) in the de Leeuw and Cooper set.[24] This assumption of transferability was examined using MD simulations of several smaller systems (below). Table S1 lists elementary aqueous and lattice species considered in our MD simulations. The parameters of the interatomic potential functions (see eqs 1 and 2) are summarized in Tables S2 and S3.

In MD simulations of the aggregation of iron molecular clusters an artificial external field (a modified version of the so-called containing sphere field on p 133 of ref 23) was applied to some MD systems (below) in order to speed up the nucleation process. This field directs the movement of atoms toward the center of the MD box, imitating the sedimentation of particles under centrifugation. The external field takes the form of

$$U_{ij}(r_c) = -A(R_0 - r_c)^3 = -(m^{1.5}A_0)(R_0 - r_c)^3 \tag{3}$$

where A (and A_0) is a parameter representing the field strength, R_0 the radius of the designed containing sphere (chosen as 25 Å in this work), and r_c the distance of an atom away from the center of the MD box. The field strength A was taken to be proportional to $m^{1.5}$ (m is the atomic weight of an atom), so that iron molecular clusters formed in a MD simulation would move faster than water molecules toward the MD box center, facilitating close approach of the clusters. Values of A_0 were chosen such that the movement of clusters was significantly enhanced without leading to breaking of bonds in previously formed aggregates.

2.2. Choice of Water Models for NPT Simulations. The shell water model[26] was used in both the de Leeuw and Cooper potential set[24] and the Spagnoli et al. potential set.[27] It has been used to study mineral surfaces in equilibrium with water.[26,27] In the prior simulations, the NVT/NVE ensemble was used for equilibration before final adjustment of the system pressure

DOI: 10.1021/acs.jpcb.5b03801
J. Phys. Chem. B 2015, 119, 10630−10642

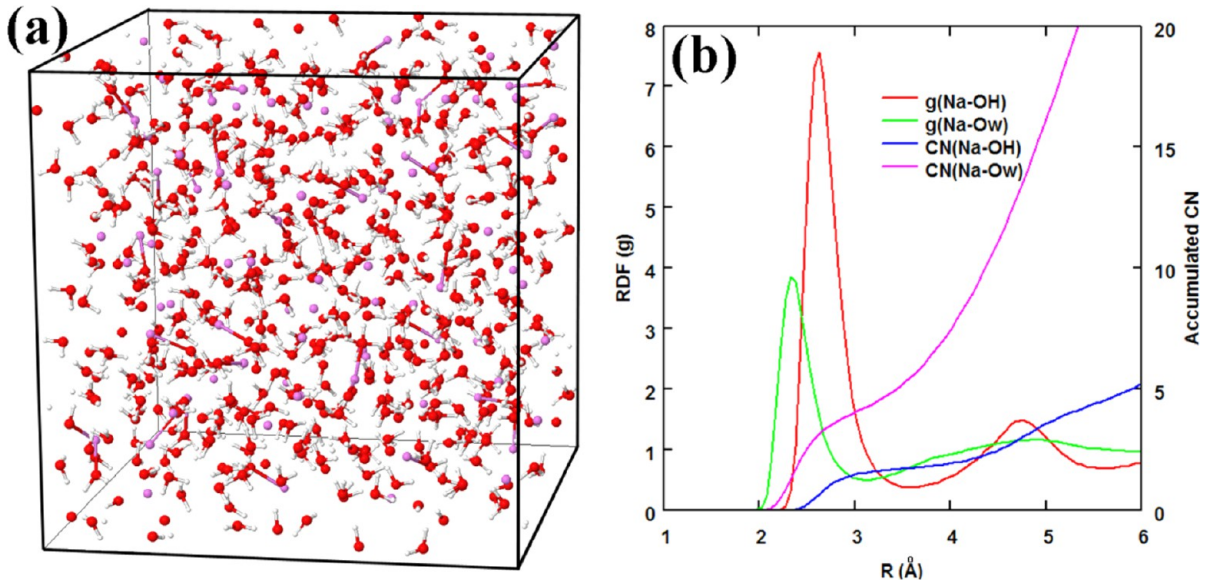

Figure 1. (a) Snapshot of an 8.5 M NaOH aqueous solution at MD time 500 ps: red, O; gray, H; violet, Na. (b) Radial distribution functions (g) and accumulated coordination numbers of atoms (CN) of hydroxyl oxygen ("OH") and water oxygen ("OW") around a sodium cation.

using the NPT ensemble.[24,27] In the present work, we are interested in the dynamics of nucleation of iron oxyhydroxide at ambient condition (300 K, 1 atm). The NPT ensemble is appropriate, while the NVT and NVE ensembles are not because their system pressures change with MD time. To examine the shell water model in NPT simulations, we ran a MD simulation of water at 300 K and 1 atm (see SI, section 3). Results show that the system volume and pressure diverge in the NPT simulation (see SI, section 3).

Alternatively, we ran a MD simulation of water using the CF1 water model in an NPT ensemble (see SI, section 3). Results show that the system reached a steady state after equilibration for ~120 ps; the T & P converged to the required values (300 K, 1 atm ≅ 0 kbar) in the steady state. On the basis of the NPT simulation behaviors of the two water models, we thus have chosen the CF1 water model for MD simulations of the nucleation of iron oxyhydroxide.

2.3. Transferability of Potential Functions. To examine the transferability of the combined potential sets (above) for MD simulations of solutions relevant to iron oxyhydroxide nucleation, the following test MD simulations were performed. Computation details are given in the SI.

a. Applicability of Ferric Ion Potentials Designed for Solid Phases to a Ferric Aqueous Solution. In the combined potential set (Tables S2 and S3, SI), the Fe^{3+}−H_2O interaction potentials were designed originally for iron cations in iron oxide and oxyhydroxide phases.[24,27] To examine their transferability to aqueous solutions, we performed a MD simulation of a system consisting of $1Fe^{3+}$ + $492H_2O$ in a MD box of initially ~$(20\ Å)^3$. An NPT simulation (300 K, 0 kbar) was run for 500 ps with a time step of 5×10^{-5} ps. The equilibrated concentration of Fe^{3+} is ~0.1 M

Results (SI, section 4) show that the MD correctly reproduced the coordination numbers (CN) of iron for the first hydration shell (CN = 6), consistent with experimental results cited in refs 7 and 9 and previous simulation results.[13,17,18] The experimental result for the CN of the second hydration shell is ~12.[7] Our simulated CN of the second shell is ~14, close to those (13.3−13.6) obtained from quantum mechanical/first-principle simulations.[13,17,18]

The average Fe−O distance is 2.20 Å in the first hydration shell (Figure S4b, SI). The experimental Fe−O bond length of hydrated ferric ions falls in the range of 1.94−2.08 Å.[17] A recent X-ray absorption study obtained an average Fe−O bond length of 1.99 Å in ferric monomers.[8] In comparison, simulated first Fe−O distances fall in the range ~1.92−2.30 Å.[9−20] Our result is close to the upper bound. Giving that the employed ferric potential was not specifically designed for aqueous solutions, we regard this result as reasonable.

The Fe−O distance in the second hydration shell peaks at ~4.42 Å (Figure S4b, SI). This agrees with the results of previous CPMD and QM/MM studies[13,18] as well as the value (4.31 Å) of the recent experimental study.[8] We noticed that the hydrated ferric iron is also hydroxylated, forming a $[Fe(H_2O)_4(OH)_2]^+$ species (Figure S4a, SI) with an average Fe−OH distance of 1.80 Å and an average Fe−OH_2 distance of 2.24 Å in the sampled structure. This species has been documented as a major component in ferric salt solutions.[31] This is reasonable, as the simulated system does not include a strongly acidic solution in which $[Fe(H_2O)_6]^{3+}$ should prevail, and thus, some degree of hydrolysis of ferric ion is expected. The OH^- groups for the hydrolysis came from the dissociation of water (CF1 model). This result shows the advantage of using a dissociable water model over nondissociation water models such as the SPC/SPCE models.

b. Applicability of the Hydroxyl Potentials Designed for Solid Phases to a NaOH Aqueous Solution. The OH^- potentials were designed originally for iron oxyhydroxide (FeOOH) solid phases.[24] To examine their transferability to aqueous solutions, we performed a MD simulation of a system containing 83NaOH + $464H_2O$ in a MD box of initially ~$(30\ Å)^3$ size. An NPT simulation (300 K, 0 kbar) was run for 500 ps with a time step of 5×10^{-5} ps. The equilibrated concentration of NaOH was ~8.5 M.

We found that it was necessary to adjust the original ρ parameter (0.3065 Å)[27] for the van der Waals interaction between Na^+ and OH^- (Table S2, SI). The ρ value (0.3350 Å)

DOI: 10.1021/acs.jpcb.5b03801
J. Phys. Chem. B 2015, 119, 10630−10642

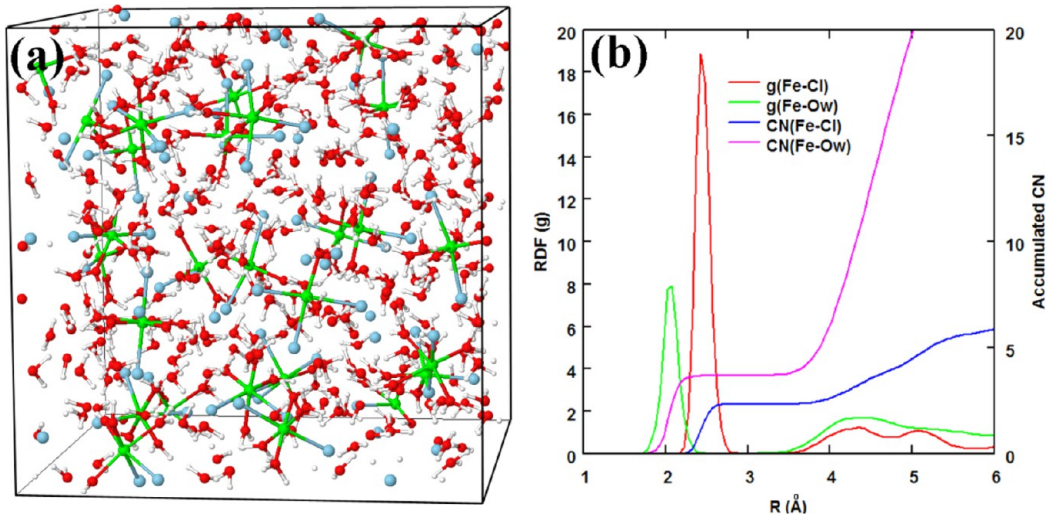

Figure 2. (a) Snapshot of a 4.1 M $FeCl_3$ aqueous solution at MD time 500 ps: red, O; green, Fe; gray, H; blue, Cl. Iron cations are coordinated by water molecules and chorine anions. (b) Radial distribution functions (g) and accumulated coordination numbers of atoms of chlorine and water oxygen around an iron cation.

Scheme 1. MD Simulated Physical Chemical Processes

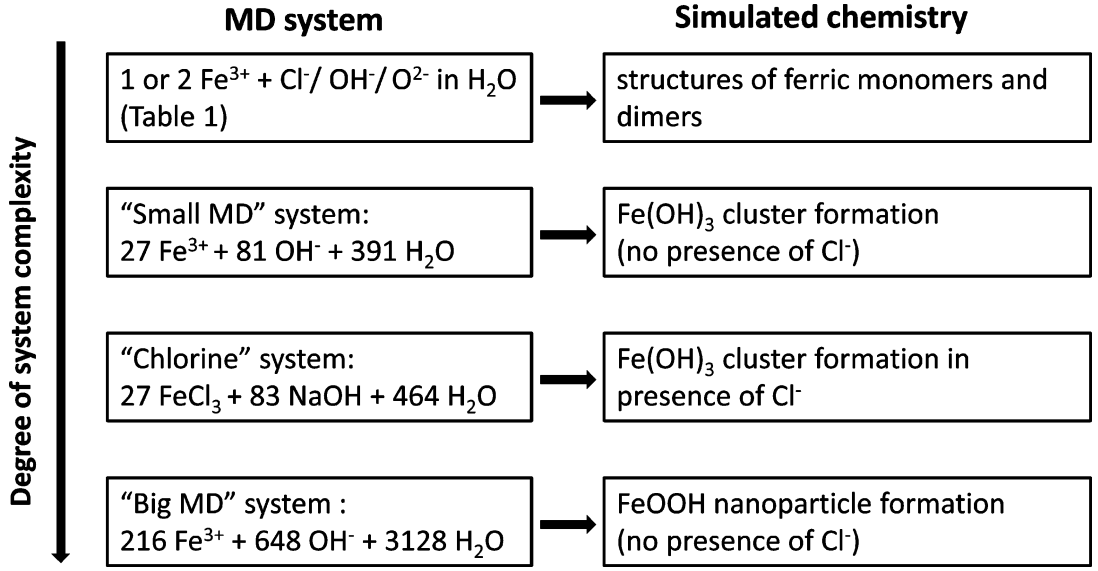

was determined such that the Na−O(hydroxyl) and Na−O(water) distances could better reproduce those from the radial distribution functions determined from neutron and X-ray scattering.[32]

Snapshots from the simulation are shown in Figure 1. Figure 1a shows that the Na^+ cations are surrounded by both water molecules and hydroxyl groups in the solution. Radial distribution functions (Figure 1b) show that the Na−O(water) distribution peaks at ∼2.35 Å, and the Na−O(hydroxyl) distribution peaks at ∼2.63 Å. The neutron scattering study showed that the Na−O(water) distance is ∼2.4 Å, insensitive to the NaOH concentration.[32] The X-ray scattering study showed that the Na−O(water) distance is ∼2.45 Å in 4.7−19.1 M NaOH solutions, and the Na−O(hydroxyl) distance is 2.50 Å in 15.4−19.1 M NaOH solutions.[33] The two Na−O distances from our simulations are in reasonable agreement with the experimental results.

c. Applicability of Ferric Ion Potentials Designed for Solid Phases to an $FeCl_3$ Aqueous Solution. To examine the transferability of the ferric ion potentials to $FeCl_3$ aqueous solutions, we performed a MD simulation of the system $27FeCl_3 + 391H_2O$ in a MD box of initially ∼(25 Å)^3 size. An NPT simulation (300 K, 0 kbar) was run for 500 ps with a time step of 5×10^{-5} ps. The equilibrated concentration of $FeCl_3$ is 4.1 M.

Figure 2a shows that in the solution, most Fe^{3+} ions are coordinated by $2Cl^-$ and $3Cl^-$ and some are by $4Cl^-$, forming iron species of $[Fe(H_2O)_4Cl_2]^+$, $[Fe(H_2O)_3Cl_3]^0$, and $[Fe(H_2O)_2Cl_4]^-$, respectively. Radial distribution functions in Figure 2b show that the Fe−O(water) distribution peaks at ∼2.05 Å and the Fe−Cl distribution at ∼2.36 Å. An X-ray scattering study[34] has shown that in 2.3−5.8 M $FeCl_3$ solutions, the major iron species are $[Fe(H_2O)_4Cl_2]^+$ and $[Fe(H_2O)_3Cl_3]^0$ and the average Fe−O(water) and Fe−Cl distances are 2.00 and 2.32 Å, respectively. Thus, our MD results are close to those from experimental work.

The above test simulation results show that the combined de Leeuw and Cooper[24] and Spagnoli et al.[27] potential sets,

DOI: 10.1021/acs.jpcb.5b03801
J. Phys. Chem. B 2015, 119, 10630−10642

though not designed specifically for aqueous solutions, performed adequately in MD simulations of ferric ion solvation and the solutions of NaOH and $FeCl_3$ when they were used with the CF1 water model after minor parameter adjustment (Table S2, SI). Therefore, we regard these potentials as reasonably transferable to aqueous solutions for MD simulations of the nucleation of iron oxyhydroxide created by the mixing of ferric ions and hydroxyl groups.

3. SIMULATION RESULTS AND DISCUSSIONS

Several MD systems with varying degree of complexity were constructed for simulating the physical chemical processes occurring when mixing ferric ions with hydroxyl groups in aqueous solutions, as illustrated in Scheme 1.

3.1. Simulation of Formation of Iron Monomers and Dimers in Dilute Solutions. Five systems with initial volumes of ~$(25\ Å)^3$ were constructed for simulations of formation of hydrated and/or hydroxylated iron monomers and dimers, as listed in Table 1. MD simulations were run for equilibrium at NPT conditions (300 K, 0 kbar) for several hundreds of picoseconds (Table 1) with a time step of 5×10^{-5} or 1×10^{-4} ps. In some systems, an "inert" chlorine anion (iCl^-) was used for charge balancing. A chlorine ion was made inert by setting up a potential hill between an Fe^{3+} ion and the Cl^- ion, which keeps the Fe^{3+}–Cl^- distance > ~6 Å and thus prevents bond formation between them. This was realized by changing the ρ parameter for the Fe–Cl pair from 0.4161 (Table S2, SI) to 1.1000 Å based on trial-and-error tests.

Table 1. MD Simulations of Iron Monomers and Dimers in Aqueous Solutions

no.	MD system (initial setup)	MD time (ps)	iron monomer/dimer formed at end of MD simulations	C[c] (M)
1	$Fe^{3+} + 3Cl^- + 494H_2O$	500	$[Fe(OH)Cl_2(H_2O)_3]$	0.1
2	$Fe^{3+} + 3iCl^-$ [a] $+ 494 H_2O$	220	$[Fe(OH)_3(H_2O)_3]$	0.1
3	$2Fe^{3+} + OH^- + 5iCl^-$ [a] $+ 531H_2O$	366	$[(H_2O)_4(OH)_2Fe{-}(OH){-}Fe(OH)(H_2O)_4]^{2+}$	0.2
4	$2Fe^{3+} + 2OH^- + 4 iCl^-$ [a] $+ 492H_2O$	437	$[(H_2O)_5Fe{-}(OH)_2{-}Fe(OH)(H_2O)_4]^{3+}$	0.2
5	$2Fe^{3+} + O^{2-}$ [b] $+ 4iCl^-$ [a] $+ 525H_2O$	435	$[(H_2O)_4(OH)Fe{-}O{-}Fe(OH)(H_2O)_4]^{2+}$	0.2

[a] iCl^-: inert Cl^- for charge balance of the MD system. [b] O^{2-}: standalone anion for the initial setup. [c] Iron concentration.

In the equilibrated MD system $Fe^{3+} + 3Cl^- + 494H_2O$ (no. 1 in Table 1), an iron monomer was formed by complexation of a ferric ion with water molecules, a hydroxyl group dissociated from water, and chlorine anions: $Fe(OH)Cl_2(H_2O)_3$. Figure S5a (SI) shows a snapshot of the system. The average Fe–Cl bond length is 2.43 Å (Figure S5b, SI), close to that (2.32 Å) found via X-ray scattering.[34] In another simulation (no. 2 in Table 1), we forced the chlorine–ferric ion distance to be longer than 6 Å (see above), preventing their complexation. This inert chlorine can be regarded as being present only to satisfy system charge balance. In this case, in the monomer, the previously coordinated chlorine ions were replaced by hydroxyls, generating an iron monomer of $Fe(OH)_3(H_2O)_3$.

When one (no. 3, Table 1) or two (no. 4, Table 1) hydroxyl groups were added to an aqueous solution containing two ferric cations (charge balanced by inert chlorine ions), μ-hydroxo(or dihydroxo)-bridged iron dimers formed: $[(H_2O)_4(OH)_2Fe{-}(OH){-}Fe(OH)(H_2O)_4]^{2+}$ and $[(H_2O)_5Fe{-}(OH)_2{-}Fe(OH){-}(H_2O)_4]^{3+}$. In these dimers, some hydroxyl groups come from the dissociation of water. This reduces the overall charge of a dimer, stabilizing the dimer structure.

In one case (no. 5, Table 1) the addition of an initially standalone oxygen anion (O^{2-}) into a MD system containing two ferric cations (charge balanced by inert chlorine ions) created a μ-oxo-bridged iron dimer.

Instantaneous structures of the iron monomers and dimers at the ends of the simulations are illustrated in Figure 3. One notes that some iron nuclei (Figures 3c and 3d) are overcoordinated (i.e., CN = 7 rather than the regular number of 6). This is because the sampled structures are dynamic: ligand water molecules are exchanging with the solvent water molecules. When one water molecule initially binds with one

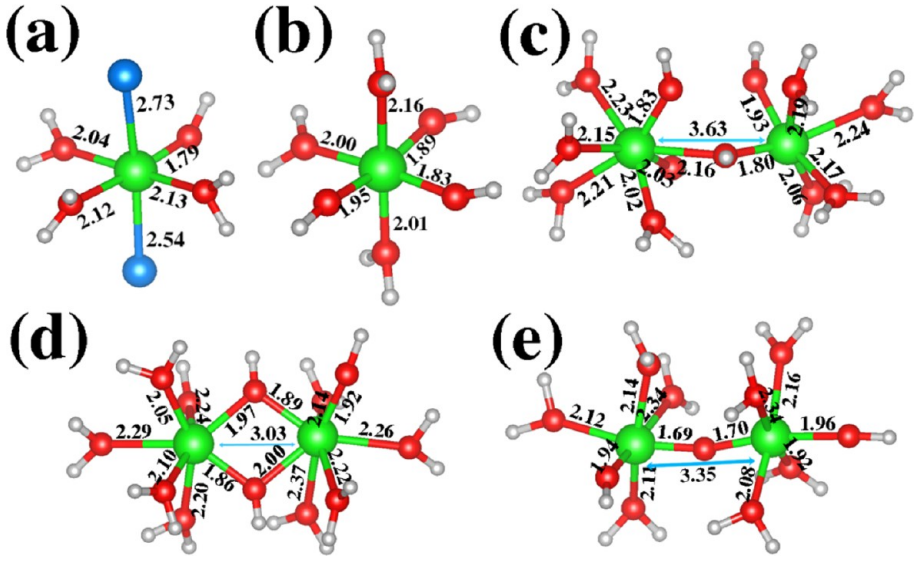

Figure 3. Structures of iron monomers (a, b) and dimers (c, d, e) sampled at the ends of MD simulations (see Table 1). a–e correspond to the MD systems 1–5 in Table 1: red, O; green, Fe; gray, H; blue, Cl.

DOI: 10.1021/acs.jpcb.5b03801
J. Phys. Chem. B 2015, 119, 10630–10642

iron nucleus while a bound ligand has not yet left the core at a sampling instance, a structure with seemingly overcoordinated nuclei is captured. Analysis of time series radial distribution functions showed that for clusters in Figures 3c and 3d, the ferric ions have CN = 6 for over 90% and 85% of the time, respectively. NMR experiments have revealed that ligand water exchange is consistent with associative activation for substitution for monomer $Fe(OH_2)_6^{3+}$ (i.e., via the associative interchange mechanism[7]) and dissociative activation for substitution for monomer $Fe(OH_2)_5(OH)^{2+}$.[35,36] However, the water exchange mechanism may be more complex for iron dimers than for monomers.

For the μ-oxo dimer in Figure 3e, the Fe−O(oxo) distance (~1.70 Å), Fe−O−Fe distance (3.35 Å), and Fe−O−Fe angle (163°) are close to those measured in a protein crystal (i.e., respectively, 1.71−1.76 Å, 3.38 Å, and 165°).[37] The average bond lengths or interatomic distances from all clusters are listed in Table 2. The average Fe−O distance in Fe−OH (1.90 Å) is shorter than the average distance in $Fe-OH_2$ (2.14 Å). This is consistent with previous computations.[11,12,16]

Table 2. Average Interatomic Distances (Angstroms) between Iron and Adjacent Atoms

molecular configuration	Fe−O(water)	Fe−O(hydroxyl)	Fe−Cl	Fe−O(oxo)	Fe−Fe
Figure 3a	2.10	1.79	2.64		
Figure 3b	2.06	1.89			
Figure 3c	2.16	1.95			3.63
Figure 3d	2.21	1.93			3.03
Figure 3e	2.15	1.95		1.70	3.35
mean (3a − 3 e)	2.14	1.90			

3.2. Simulation of the Formation of Iron Hydroxide ($Fe(OH)_3$) Clusters (no presence of chlorine). A "Small MD" system containing $27Fe^{3+}$ + $81OH^-$ + $391H_2O$ in a MD box of initially ~$(25\ Å)^3$ was constructed for simulation of iron hydroxide formation in an aqueous solution. This system approximately simulates the neutralization of ferric ions by hydroxyl groups in aqueous solutions without other specific anion−ferric interactions (such as Cl−Fe), which might be assumed for the reaction of ferric nitrate and sodium hydroxide. As potential functions compatible with those used in this work are not available for nitrate anions, explicit inclusion of NO_3^- in our MD simulations was not considered. MD simulation of this system was run at NPT conditions (300 K, 0 kbar) for 55.3 ns with a time step of 5×10^{-5} ps. The concentration of $Fe(OH)_3$ in the equilibrated system is ~3.6 M.

During the structure evolution of the Small MD system, we observed the formation of molecular clusters of iron hydroxide, the aggregation and occasional disaggregation of molecular clusters, and the densification of the aggregated clusters. Snapshots of the MD system at different times are displayed in Figure S6 (SI); some are shown in Figure 4. Dynamic processes that occurred in the system can be viewed in a MD movie that is accessible online (link included in the SI).

Results show that upon mixing of Fe^{3+} and OH^- in water (Figure 4a), OH^- groups move quickly and bind with Fe^{3+} ions, forming iron−hydroxyl monomers. These monomers diffuse and then merge to form dimers after ~10 ps and trimers and oligomers (Figure 4b) after ~50 ps due to the strong affinity of ferric ions for the hydroxyls. The formed iron molecular clusters further join through chain formation and branching, resulting in larger molecular networks (Figure S6, SI). At MD time of ~10 ns, small crystalline structures characteristic of linked Fe−OH rings starts to form (Figure 4c), and these may serve as the nuclei for iron hydroxide crystals. Continuing addition of the small clusters to the nuclei leads to the formation of a two-dimensional (2D)-like nanocrystal (Figure 4d). In this crystal, most Fe atoms are coordinated by six OH^- groups (sometimes one or two of them are replaced by H_2O), forming Fe−O octahedra. These octahedra are linked together via edging sharing, producing a six-membered ring-like layered structure (Figure 4d).

The layered structure is comparable to those present in the gibbsite and bayerite phases of $Al(OH)_3$ (Figure 5). However, a bulk $Fe(OH)_3$ phase allomeric to gibbsite or bayerite has not yet been reported. This may be because $Fe(OH)_3$ has a much stronger tendency to deprotonate than $Al(OH)_3$ because Fe^{3+} is a much stronger Lewis acid (its pK_a = 2.2) than Al^{3+} (pK_a = 5.0).[38] This would readily convert $Fe(OH)_3$ to FeOOH during and following postnucleation, making it hard to detect experimentally. Radial distribution functions of the system (Figure 6) show that there are two peaks for the pair Fe−O(hydroxyl) at 1.70 and 1.91 Å, respectively. The shorter distance corresponds to the pairs at the edges of the 2D nanocrystal (Fe with CN of 5 or 4) and the longer one to the majority of the pairs (Fe with CN of 6) in the bulk of the nanocrystal. The Fe−Fe distance is ~3.05 Å, close to those in edge-sharing Fe−O octahedra in solid phases of hematite (2.89 and 2.97 Å) and goethite (3.02 and 3.29 Å), indicating that the 2D nanocrystal comprised mainly of edge-sharing Fe−O octahedra.

3.3. Simulation of Formation of Iron Hydroxide ($F(OH)_3$) Clusters in the Presence of Chlorine. In aqueous solutions, chlorine anions dissociated from a NaCl salt may produce specific interactions with ferric ions as they can coordinate with the cations, forming iron−chlorine complexes. Thus, Cl^- may affect the formation behavior of iron hydroxide in a salt solution. To study this anion effect, we constructed a "Chlorine" system consisted of $27FeCl_3$ + $83NaOH$ + $464H_2O$ in a MD box of initially ~$(30\ Å)^3$. MD simulation was run at NPT conditions (300 K, 0 kbar) for 24.8 ns with a time step of 5×10^{-5} ps. The concentration of $Fe(OH)_3$ in the equilibrated system is ~2.9 M.

Snapshots of the system at different MD time are displayed in Figure S7 (SI). A few representative examples are shown in Figure 7. The dynamic processes that occurred in the system can be viewed in a MD movie that is accessible online (link included in the SI).

Results show that upon mixing of Fe^{3+}, Cl^-, Na^+, and OH^- in water (Figure 7a), together with H_2O and OH^-, Cl^- anions quickly bind with Fe^{3+} to form six-ligand-coordinated ferric monomers. These monomers ultimately merge to form dimers, trimers, and polymers (Figure 7b). In these merging processes, chlorine anions dissociate from the iron nuclei and go into the nearby solution (see MD movie in the SI). This observation is consistent with previous experimental studies.[3,4] The molecular clusters of different sizes then join to form larger aggregates that exist mainly in the form of chains (Figure 7c). Although similar short molecular chains also form in the Small MD system without chlorine (section 3.2), when chlorine is present the chains do not aggregate to form the ring-like layered structures. This is probably because during larger cluster formation, the electric fields produced by Cl^- anions in the vicinity of the clusters prevent their lateral aggregation to form

DOI: 10.1021/acs.jpcb.5b03801
J. Phys. Chem. B 2015, 119, 10630−10642

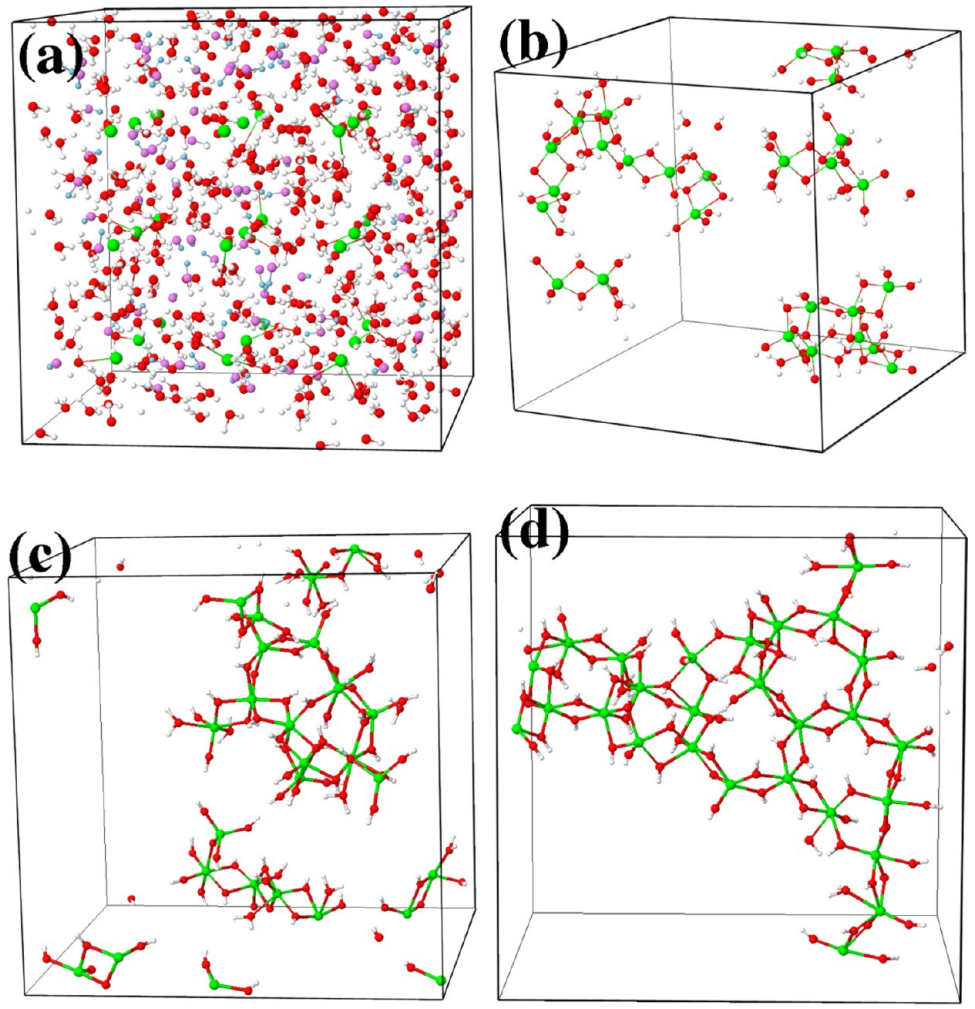

Figure 4. Initial setup of the Small MD system $27Fe^{3+}$ + $81OH^-$ + $391H_2O$ (a), and snapshots of iron molecular clusters formed at different MD time: (b) 6.5, (c) 10.0, and (d) 55.3 ns. Red, O; gray, H; green, Fe. (a) O and H atoms in hydroxyls (OH^-) were colored, respectively, violet and blue; (b–d) bulk water molecules were removed for clarity.

six-membered ring-like network structures (as in Figure 4d). The chain-like iron molecular clusters eventually tend to form a closed structure (Figure 7d), resembling the channel structure in akaganeite. Such a closed structure may serve as a precursor for the formation of akaganeite, in line with the suggestion from X-ray absorption studies.[3,4]

Radial distribution functions at the MD time 24.8 ns (Figure 8) indicate that in the iron molecular clusters, Fe^{3+} ions are coordinated and linked mainly by OH^-, with an average Fe–O (hydroxyl) bond length of 1.86 Å and a coordination number of 4.8 by OH^-. Some Fe^{3+} ions are coordinated by H_2O, with an average Fe–O(water) bond length of 2.26 Å and a coordination number of 1.3. The Fe–Fe distance is ~3.03 Å, indicating the clusters are comprised mainly of edge-sharing Fe–O octahedra (see above).

3.4. Simulation of the Formation of Iron Oxyhydroxide (FeOOH) Nanoparticles (no presence of chlorine). For simulation of the aggregation of iron molecular clusters that eventually leads to nucleation and formation of nanoparticles, a bigger MD system containing many iron cations is needed. For this, the Small MD system (section 3.2) evolved to the MD time of 10.5 ns was duplicated 2 × 2 × 2 times along the *x*, *y*, and *z* directions, forming a "Big MD" system with a volume of ~$(47\ Å)^3$ and containing 8 times the numbers of the atoms, i.e., 216 Fe^{3+} + 648 OH^- + 3128 H_2O.

MD simulations were performed in several stages, aimed at speeding up aggregation of the iron molecular clusters that formed (see Table 3). These include cases with application of higher temperature and/or pressure and use of an artificial external field (see above). For formation of iron oxyhydroxide from iron hydroxide, deprotonation (removal of protons H^+ from the OH^- groups) of the iron hydroxide clusters is needed, as shown by the following reaction

$$Fe(OH)_3 = FeOOH + H_2O \quad (4)$$

In the reaction, 1/3 of the OH^- groups (i.e., 1 OH^-) are deprotonated and the freed H^+ combines with another 1/3 of the OH^- groups (i.e., 1 OH^-) to form one H_2O. For this reason, this reaction may also be called dehydration. Since this reaction involves bond breaking and rearrangement, it could not be simulated by our CMD since the potential sets used (Tables S2 and S3, SI) are not reactive force fields. Hence, at a certain MD stage, we introduced a one-time manual deprotonation of the iron hydroxide clusters formed earlier (Table 3). Two typical percentages (33.3% and 40.0%) of the hydroxyl groups contained in the iron hydroxide clusters were randomly deprotonated, generating two Big MD systems for

DOI: 10.1021/acs.jpcb.5b03801
J. Phys. Chem. B 2015, 119, 10630–10642

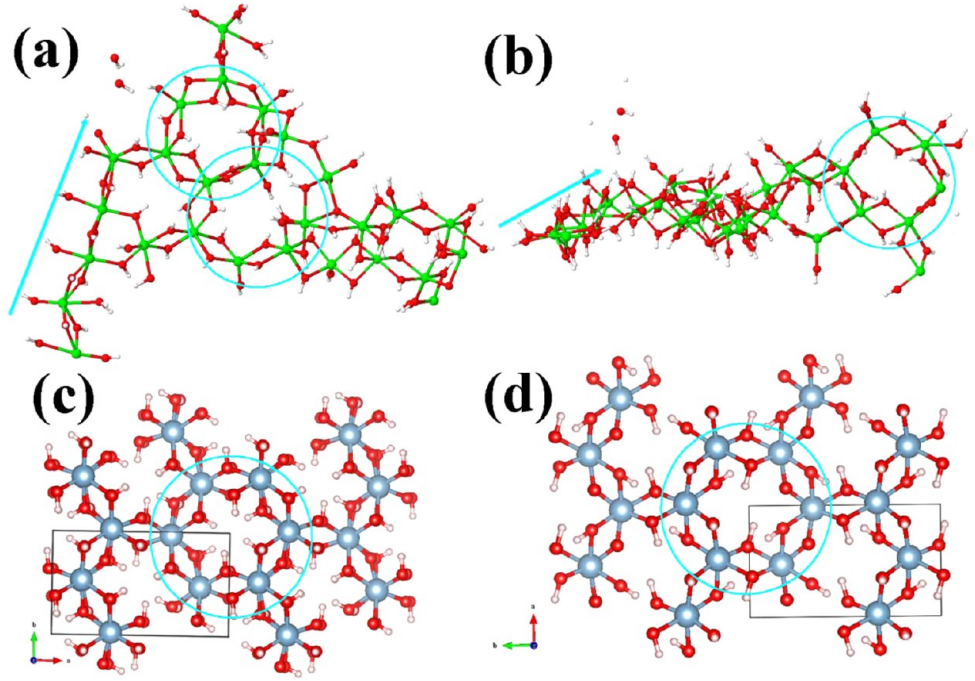

Figure 5. Chain (indicated by a blue arrow) and ring (indicated by blue circles) structured Fe−OH molecular clusters formed at 55.3 ns in the Small MD system, in top view (a) and side view (b), compared to the layered ring structures of $Al(OH)_3$ in gibbsite (c) and bayerite (d) phases. (a and b) Red, O; gray, H; green, Fe. (c and d) Red, O; light pink, H; steel blue, Al.

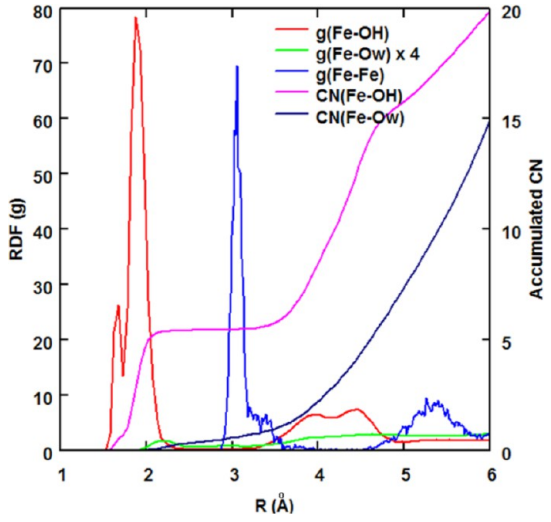

Figure 6. Radial distribution functions (g) and accumulated coordination numbers of atoms (CN) of several species around an iron cation in the Small MD system $27Fe^{3+}$ + $81OH^-$ + $391H_2O$ at 55.3 ns.

subsequent simulations (Table 3). The Big MD1 system corresponds to a complete reaction 4 (i.e., it deprotonated 1/3OH^- in $Fe(OH)_3$), while the Big MD2 corresponds to 60% of reaction 4 and 40% of the following reaction 5 (as explained below)

$$2Fe(OH)_3 = Fe_2O_3 + 3H_2O \quad (5)$$

In reaction 5, 50% of the OH^- groups (i.e., $3OH^-$) are deprotonated and the freed $3H^+$ combine with the other 50% of OH^- (i.e., $3OH^-$) to form $3H_2O$. Hence, in the Big MD2 system, the deprotonation percentage 40% comes from 0.60 × 33.3% (reaction 4) + 0.40 × 50% (reaction 5). It is apparent that the Big MD2 system has a higher degree of dehydration than the Big MD1 system.

Simulations were conducted at NPT conditions using a time step of 1×10^{-4} ps. The accumulated MD time is 17.8 ns for the Big MD1 system and 16.4 ns for the Big MD2 system (Table 3). The concentration of iron (in the form of $Fe(OH)_3$ or FeOOH) in both equilibrated systems is ∼3.5 M. Snapshots of the MD system before and after a manual deprotonation are displayed in Figures S8−S10 (SI). Representative snapshots are shown in Figure 9.

We observed that aggregation of the initial clusters (i.e., those from an expansion of the small MD time at 10.5 ns; Figure 9a) occurs as the MD simulation proceeds. However, the aggregation of clusters was relatively slow due to involvement of large number of atoms in the clusters. Thus, at MD stage 2 (Table 3), a higher temperature (T = 500 K) and pressure (P = 10 kbar) were used to speed up the cluster aggregation (Figure S8, SI) by enhancing the kinetics and creating more favorable energetics (as aggregation reduces system volume), respectively. Previously, a high-TP condition was shown to enhance cluster formation in NaCl aqueous solutions.[39] The aggregate formed at our higher T/P was relaxed at 300 K and ambient pressure (Figure 9b; Figure S8). This aggregate features a more three-dimensional (3D)-like network of Fe−O octahedra linked via edge sharing (Figure 9b). In some parts of the network (e.g., the area around the upper left corner of Figure 9b), six-membered ring-like layered structures formed, similar to those observed in the small MD system (Figure 4d).

Deprotonation of 33.3% and 40.0% of the OH^- groups in the iron molecular clusters (aggregates) led to conversion of the chemical stoichiometry from $Fe(OH)_3$ to FeOOH (Big MD1 system) and FeOOH + Fe_2O_3 (Big MD2 system), respectively (see above). These reactions are necessary in order to simulate the formation of iron oxyhydroxide/oxide nanoparticles.

DOI: 10.1021/acs.jpcb.5b03801
J. Phys. Chem. B 2015, 119, 10630−10642

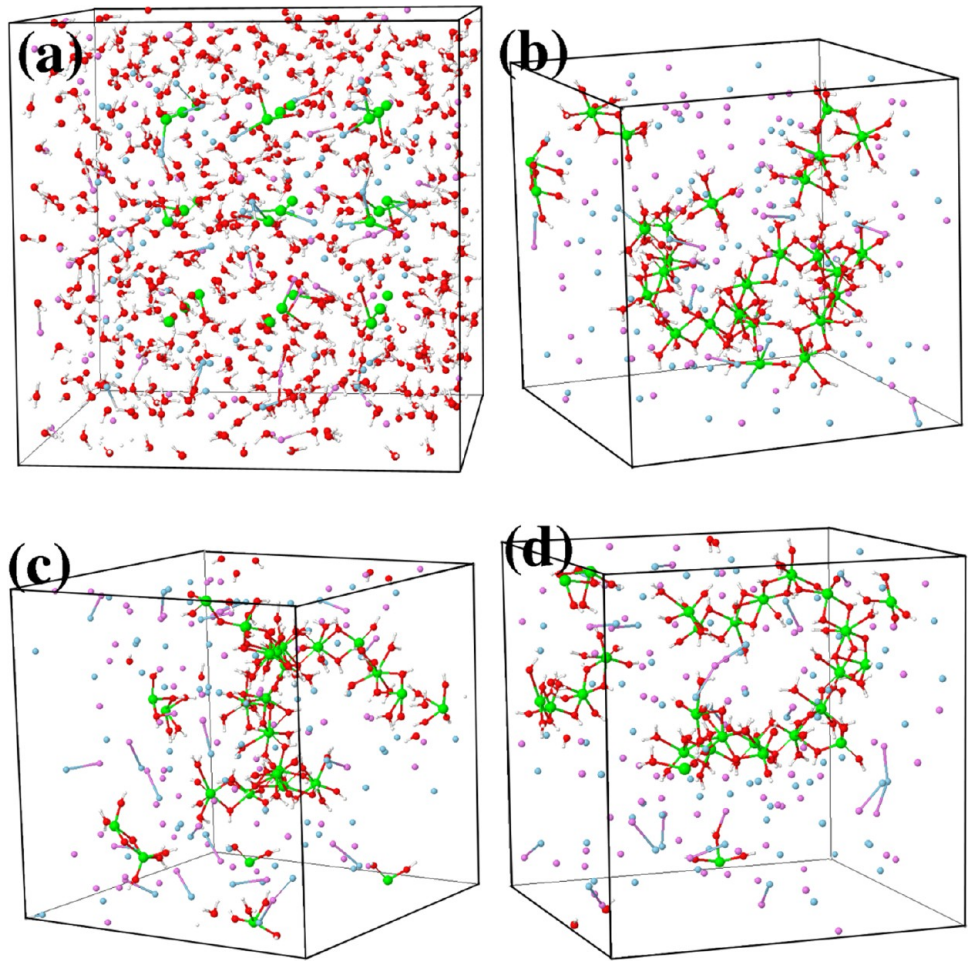

Figure 7. Initial setup of the MD system $27FeCl_3$ + $83NaOH$ + $464H_2O$ (a), and snapshots of iron molecular clusters formed at different MD time: (b) 0.5, (c) 9.2, and (d) 24.8 ns. (b–d) Bulk water molecules were removed for clarity. Red, O; gray, H; green, Fe; violet, Na; blue, Cl.

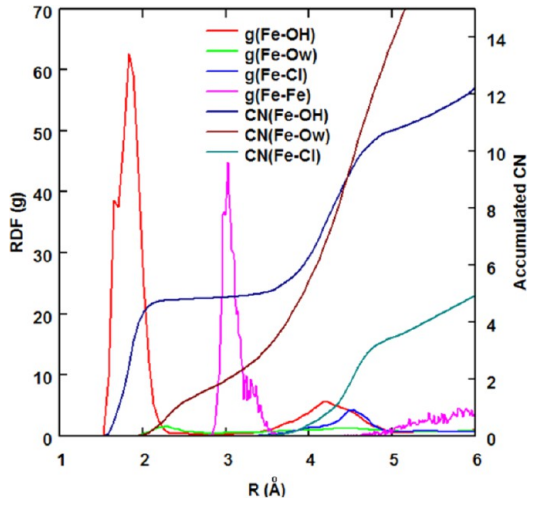

Figure 8. Radial distribution functions (g) and accumulated coordination numbers of atoms (CN) of several species around an iron cation in the MD system $27FeCl_3$ + $83NaOH$ + $464H_2O$ at 24.8 ns.

Table 3. Stages Experienced in Simulating Nanoparticle Formation in the Big MD System ($216Fe^{3+}$ + $648OH^-$ + $3128H_2O$)

stage	MD condition and time	
1	300 K, 0 kbar, 2.23 ns	
2	500 K, 10 kbar, 4.68 ns	
3	300 K, 0 kbar, 2.65 ns	
4	simulation system Big MD1: deprotonating 33.3% OH^- (one time event)	simulation system Big MD2: deprotonating 40.0% OH^- (one time event)
5	300 K, 0 kbar, 3.47 ns	300 K, 0 kbar, 3.37 ns
6	external field,[a] 300 K, 5 kbar, 2.12 ns	external field,[b] 300 K, 5 kbar, 2.03 ns
7	300 K, 5 kbar, 0.11 ns	300 K, 5 kbar, 0.13 ns
8	300 K, 1.5 kbar, 0.21 ns	300 K, 1.5 kbar, 0.21 ns
9	300 K, 0 kbar, 2.28 ns	300 K, 0 kbar, 1.06 ns
total MD time	17.75 ns	16.36 ns

[a]Under an external field with strength parameter $A_0 = 1.602 \times 10^5$ J/m^3 for 1.91 ns and then a field with $A_0 = 3.204 \times 10^5$ J/m^3 for 0.21 ns. [b]Under an external field with $A_0 = 8.010 \times 10^4$ J/m^3 for 1.82 ns and then a field with $A_0 = 3.204 \times 10^5$ J/m^3 for 0.21 ns.

The two deprotonated systems were run for ~3.5 or ~3.4 ns at ambient conditions, and cluster aggregation was observed to be still relatively slow (i.e., for most of the MD time, the clusters were just approaching each other). In order to induce appreciable aggregation formation in attainable MD time, we applied external force fields to enhance the aggregation kinetics (Table 3). A weaker external force field was insufficient to induce enough aggregation of the deprotonated clusters to

DOI: 10.1021/acs.jpcb.5b03801
J. Phys. Chem. B 2015, 119, 10630–10642

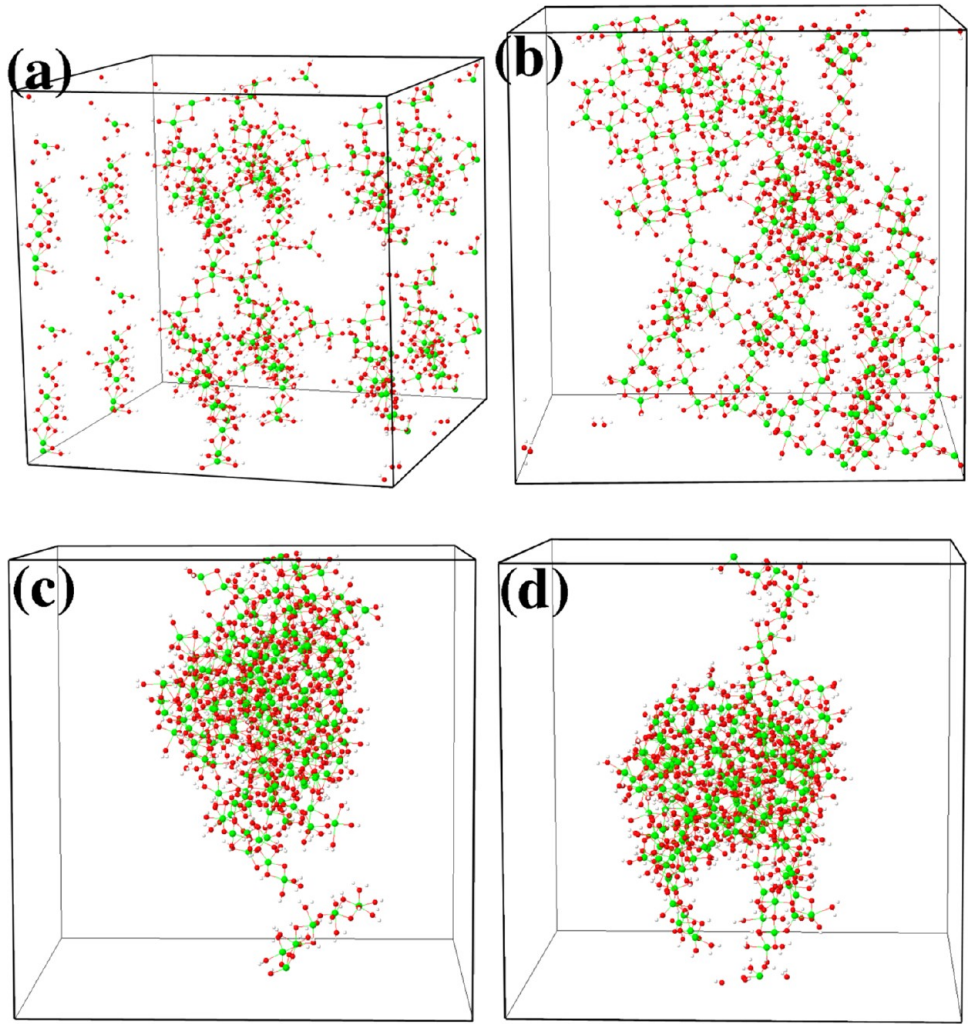

Figure 9. Initial setup of the Big MD system $216Fe^{3+}$ + $648OH^-$ + $3128H_2O$ (a), and snapshots of iron molecular clusters formed at different MD time: (b) 9.56, (c) 17.75 (Big MD 1), and (d) 16.36 ns (Big MD 2). Bulk water molecules were removed for clarity. Red, O; gray, H; green, Fe.

form nanoparticles (Table 3). Thus, stronger external fields at 5 kbar pressure were employed (stage 6, Table 3), which caused faster aggregation of the loose aggregates and formation of nanoparticles (Figures S9 and S10). After this step the nanoparticle structures experienced several stages of relaxation after removal of the external field. Snapshots of the last stages, after re-equilibration at 300 K and ambient pressure, are shown in Figures 9c and 9d for the two deprotonated systems.

The atomic structures of the nanoparticles from the two Big MD systems are compared to that of a 2 nm ferrihydrite model[40] particle (unrelaxed) in Figure 10. Unlike the ferrihydrite model structure, the nanoparticles are obviously amorphous and highly distorted. However, all three structures contain 4-, 5-, and 6-coodinated Fe atoms. The 5-coordinated Fe atoms in the model particle are located on the surfaces due to structure truncation, while in the MD amorphous particles, they may also be located in the particle interior due to the low density, though preferably on the NP surface. The distributions of the Fe and O coordination numbers are depicted in Figure 11. It is seen that, though not exactly the same, the Fe and O coordination number distributions in the MD nanoparticles and the ferrihydrite model do show similarities in terms of the dominant Fe−O polyhedral types present.

The similarity between the MD nanoparticles and the ferrihydrite model particle was further analyzed by comparing their simulated XRD patterns and atomic pair distribution functions (PDF; see, e.g., ref 41) (Figure 12). It is seen that the XRD and PDF of the 2D nanocrystal formed in the Small MD system (without introduction of deprotonation) at 55.3 ns are quite different from those of the ferrihydrite model particle. On the other hand, those of the nanoparticles formed after deprotonation in the two Big MD systems resemble those of the ferrihydrite model particle. The two PDF peaks at ∼3.0 and 3.4 Å are due to the Fe−Fe edge sharing and corner sharing of the Fe−O octahedra, respectively, in the particles. These show that the local atomic structures of the MD-generated nanoparticles are similar to that found in ferrihydrite. By comparison, in other iron oxyhydroxide phases such as goethite and lepidocrocite, the Fe−Fe edge sharing peak (at ∼3 Å) is much more pronounced than that in ferrihydrite. Therefore, we infer that during neutralization of ferric ions by hydroxyls, ferrihydrite-like nanoparticles form from a series of iron molecular clusters that deprotonate and aggregate.

3.5. Nucleation of Iron Hydroxide/Oxyhydroxide Nanoparticles via Nonclassical Pathway. In classical nucleation theory (CNT), the nucleation process is viewed as addition of ions (or ionic pairs) to the critical nuclei formed via

DOI: 10.1021/acs.jpcb.5b03801
J. Phys. Chem. B 2015, 119, 10630−10642

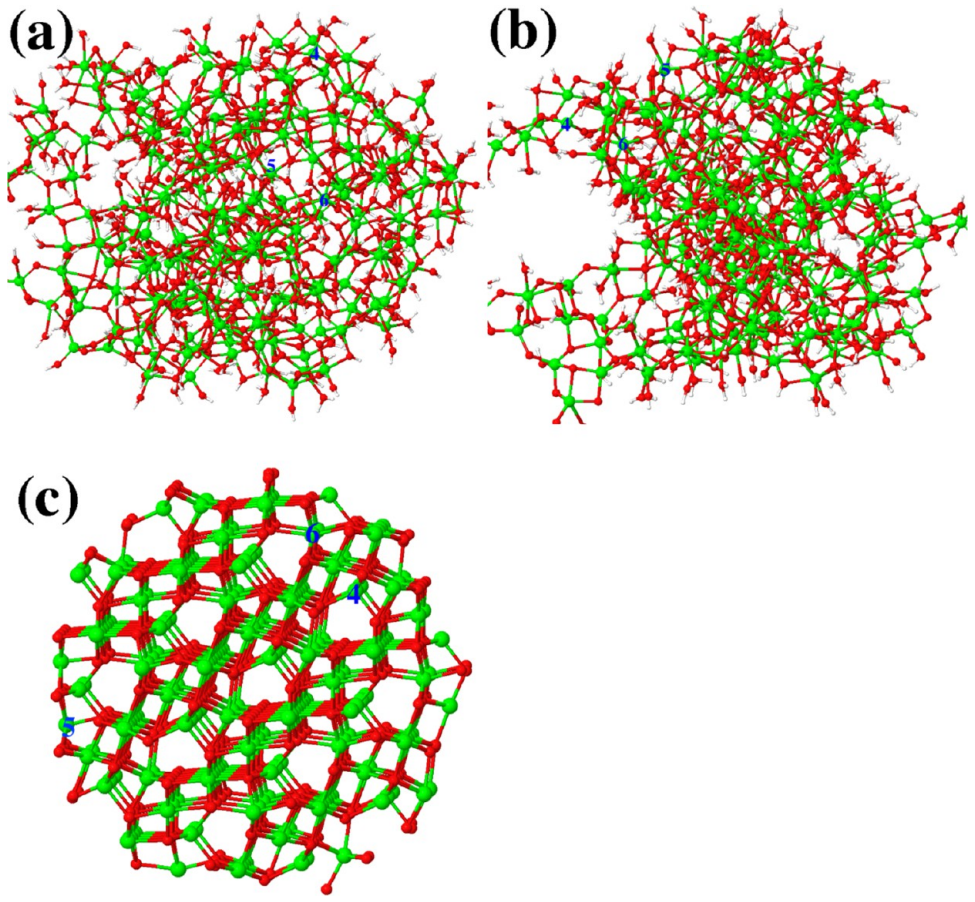

Figure 10. Structures of aggregated iron molecular clusters at the end of the simulation in Big MD 1 (a) and Big MD2 (b) compared to that of a 2 nm ferrihydrite model[40] particle (c). Blue numbers indicate coordination numbers of the underlying iron atoms. Red, O; gray, H; green, Fe.

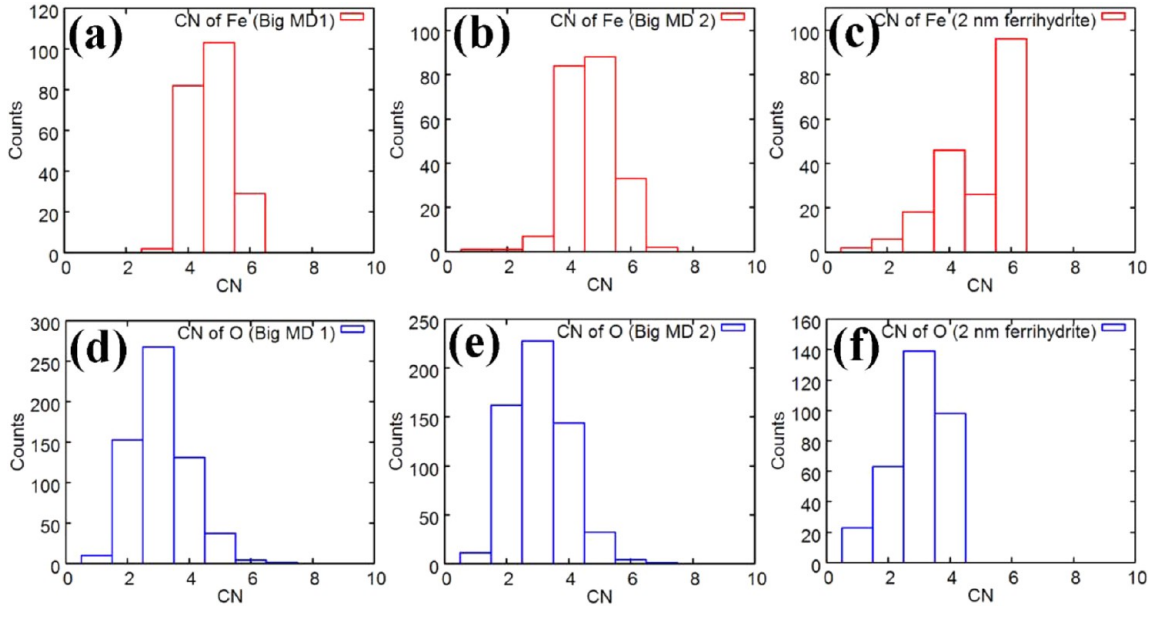

Figure 11. Coordination number distributions of Fe (a–c) and O (d–f) in aggregated iron molecular clusters formed at the end of the simulation in Big MD1 (a, d) and Big MD2 (b, e) and in a 2 nm ferrihydrite model[40] particle (c, f).

thermal fluctuation. When the particles are larger than the critical nucleus size, they can grow spontaneously. In contrast, Gebauer et al. observed that nucleation of calcium carbonate particles in aqueous solutions can proceed via aggregation of thermodynamically stable (with respect to the parent solution) prenuclei clusters,[42] whose sizes are in the range of ∼2–6 nm.[43] This pathway of nucleation is called nonclassical nucleation (with respect to CNT).[43,44] Our simulation results above

DOI: 10.1021/acs.jpcb.5b03801
J. Phys. Chem. B 2015, 119, 10630–10642

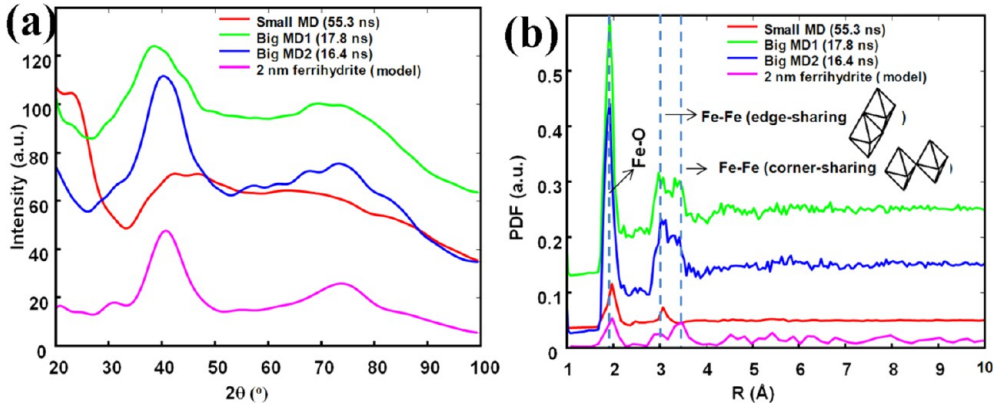

Figure 12. Simulated XRD patterns (λ = 1.7903 Å) (a) and pair distribution functions (b) of iron molecular clusters produced by MD simulations and a 2 nm ferrihydrite model[40] particle.

showed that iron hydroxide/oxyhydroxide nanoparticles form through of a series of molecular cluster formation and subsequent/concurrent cluster aggregation. In view of this, the nucleation of hydroxide/oxyhydroxide nanoparticles in our simulations adopts a nonclassical pathway. Recently, Baumgartner et al. found that growth of magnetite nanoparticles proceeded via rapid accretion of primary clusters that have sizes of ~1 nm.[45] Whether the primary clusters are prenuclei clusters was not identified.[44] Our simulation results for the system $FeCl_3$ + NaOH, which is the same as that in ref 45, suggest that the experimentally observed primary clusters might have been formed via aggregation of iron molecular monomers, dimers, and oligomers. Thus, they could be called prenuclei clusters.

4. CONCLUSIONS

MD simulations of neutralization of ferric ions in aqueous solutions have revealed the dynamic processes of formation of iron molecular clusters and the steps in their transformation to nanoparticles. In systems where anions (except hydroxyl) have no specific interactions with ferric ions, including the system containing $27Fe^{3+}$ + $81OH^-$ + $391H_2O$ and the system containing 216 Fe^{3+} + 648 OH^- + 3128 H_2O prior to deprotonation, iron monomers form by complexation of ferric ions with water molecules and hydroxyl groups. This is followed by merging to form dimers, trimers, and other oligomers, driven by molecular diffusion and strong affinity of ferric ions to hydroxyls. These units continue to aggregate, ultimately forming larger clusters with six-membered ring-like layered structures that are allomeric to aluminum hydroxide phase gibbsite or bayerite. In cases of deprotonation accompanying cluster polymerization and aggregation (e.g., in the system containing $216Fe^{3+}$ + $648OH^-$ + $3128H_2O$ after deprotonation), amorphous iron oxyhydroxide nanoparticles are predicted to form from aggregate agglomeration. These have local atomic structures and X-ray scattering patterns similar to those of small ferrihydrite nanoparticles.

In a system containing chlorine anions, water molecules, and hydroxyls, chlorine anions coordinate first with ferric ions to form monomers that merge to form polynuclei iron molecular clusters while the chlorine anions dissociate from the complex simultaneously. In contrast to the systems without specific anion−iron interactions, the iron molecular clusters in the chlorine system aggregate and form long chain-like structures that may ultimately serve as a precursor for akaganeite formation rather than ferrihydrite. These molecular processes may be very relevant to neutralization of acidic, iron-rich solutions such as those formed by alteration of mineral deposits (e.g., acid mine drainage or weathering reactions). They also give insight into the possible physical and chemical processes that are important during nucleation and growth of iron oxyhydroxides from aqueous solutions. Most notable is the predicted role of cluster aggregation[43] rather than monomer addition, as would be expected in classical growth models.

■ ASSOCIATED CONTENT

Ⓢ Supporting Information

The Supporting Information is available free of charge on the ACS Publications website at DOI: 10.1021/acs.jpcb.5b03801.

MD species, force field parameters, tests of water models, simulated hydration shells of a ferric ion, simulated complexation of a ferric ion by chlorine, snapshots of several MD systems, and MD movies showing dynamics of ion molecular cluster formation (PDF)

■ AUTHOR INFORMATION

Corresponding Author

*E-mail: heng@eps.berkeley.edu.

Notes

The authors declare no competing financial interest.

■ ACKNOWLEDGMENTS

This research was supported primarily by the U.S. Department of Energy (DOE), Office of Science, Basic Energy Sciences (BES), under Award no. DE-AC02-05CH11231, and by the National Science Foundation (NSF), under Award no. CHE-1213835. We thank Drs. M. Zhu and B. Legg for helpful discussions.

■ REFERENCES

(1) Cornell, R. M.; Giovanoli, R.; Schneider, W. Review of the Hydrolysis of Iron(III) and the Crystallization of Amorphous Iron(III) Hydroxide Hydrate. *J. Chem. Technol. Biotechnol.* **1989**, *46*, 115−134.

(2) Rose, J.; Manceau, A.; Masion, A.; Bottero, J.-Y. Structure and Mechanisms of Formation of $FeOOH(NO_3)$ Oligomers in the Early Stages of Hydrolysis. *Langmuir* **1997**, *13*, 3240−3246.

(3) Combes, J. M.; Manceau, A.; Calas, G.; Bottero, J. Y. Formation of Ferric Oxides from Aqueous Solutions: A Polyhedral Approach by X-Ray Absorption Spectroscopy: I. Hydrolysis and Formation of Ferric Gels. *Geochim. Cosmochim. Acta* **1989**, *53*, 583−594.

DOI: 10.1021/acs.jpcb.5b03801
J. Phys. Chem. B 2015, 119, 10630−10642

(4) Bottero, J. Y.; Manceau, A.; Villieras, F.; Tchoubar, D. Structure and Mechanisms of Formation of Iron Oxide Hydroxide (Chloride) Polymers. *Langmuir* **1994**, *10*, 316−319.
(5) Zhu, M.; Legg, B.; Zhang, H.; Gilbert, B.; Ren, Y.; Banfield, J. F.; Waychunas, G. A. Early Stage Formation of Iron Oxyhydroxides during Neutralization of Simulated Acid Mine Drainage Solutions. *Environ. Sci. Technol.* **2012**, *46*, 8140−8147.
(6) Hu, Y.; Lee, B.; Bell, C.; Jun, Y.-S. Environmentally Abundant Anions Influence the Nucleation, Growth, Ostwald Ripening, and Aggregation of Hydrous Fe(III) Oxides. *Langmuir* **2012**, *28*, 7737−7746.
(7) Ohtaki, H.; Radnai, T. Structure and Dynamics of Hydrated Ions. *Chem. Rev.* **1993**, *93*, 1157−1204.
(8) Zhu, M.; Puls, B. W.; Frandsen, C.; Kubicki, J. D.; Zhang, H.; Waychunas, G. A. In Situ Structural Characterization of Ferric Iron Dimers in Aqueous Solutions: Identification of μ-Oxo Species. *Inorg. Chem.* **2013**, *52*, 6788−6797.
(9) Curtiss, L. A.; Halley, J. W.; Hautman, J.; Rahman, A. Nonadditivity of *ab inito* Pair Potentials for Molecular Dynamics of Multivalent Transition Metal Ions in Water. *J. Chem. Phys.* **1987**, *86*, 2319−2327.
(10) Guardia, E.; Padro, J. A. Molecular Dynamics Simulation of Ferrous and Ferric Ions in Water. *Chem. Phys.* **1990**, *144*, 353−362.
(11) Martin, R. L.; Hay, P. J.; Pratt, L. R. Hydrolysis of Ferric Ion in Water and Conformational Equilibrium. *J. Phys. Chem. A* **1998**, *102*, 3565−3573.
(12) Lopes, L.; de Laat, J.; Legube, B. Charge Transfer of Iron(III) Monomeric and Oligomeric Aqua Hydroxo Complexes: Semiempirical Investigation into Photoactivity. *Inorg. Chem.* **2002**, *41*, 2505−2517.
(13) Remsungnen, T.; Rode, B. M. QM/MM Molecular Dynamics Simulation of the Structure of Hydrated Fe(II) and Fe(III) Ions. *J. Phys. Chem. A* **2003**, *107*, 2324−2328.
(14) Remsungnen, T.; Rode, B. M. Molecular Dynamics Simulation of the Hydration of Transition Metal Ions: The Role of Non-Additive Effects in the Hydration Shells of Fe^{2+} and Fe^{3+} Ions. *Chem. Phys. Lett.* **2004**, *385*, 491−497.
(15) Amira, S.; Spångberg, D.; Probst, M.; Hermansson, K. Molecular Dynamics Simulation of Fe^{2+}(aq) and Fe^{3+}(aq). *J. Phys. Chem. B* **2004**, *108*, 496−502.
(16) De Abreu, H. A.; Guimarães, L.; Duarte, H. A. Density-Functional Theory Study of Iron(III) Hydrolysis in Aqueous Solution. *J. Phys. Chem. A* **2006**, *110*, 7713−7718.
(17) Bogatko, S. A.; Bylaska, E. J.; Weare, J. H. First Principles Simulation of the Bonding, Vibrational, and Electronic Properties of the Hydration Shells of the High-Spin Fe^{3+} Ion in Aqueous Solutions. *J. Phys. Chem. A* **2010**, *114*, 2189−2200.
(18) Moin, S. T.; Hofer, T. S.; Pribil, A. B.; Randolf, B. R.; Rode, B. M. A Quantum Mechanical Charge Field Molecular Dynamics Study of Fe^{2+} and Fe^{3+} Ions in Aqueous Solutions. *Inorg. Chem.* **2010**, *49*, 5101−5106.
(19) Rustad, J. R.; Hay, B. P.; Halley, J. W. Molecular Dynamics Simulation of Iron(III) and its Hydrolysis Products in Aqueous Solution. *J. Chem. Phys.* **1995**, *102*, 427−431.
(20) Amira, S.; Spångberg, D.; Zelin, V.; Probst, M.; Hermansson, K. Car-Parrinello Molecular Dynamics Simulation of Fe^{3+}(aq). *J. Phys. Chem. B* **2005**, *109*, 14235−14242.
(21) Panina, N. S.; Belyaev, A. N.; Eremin, A. V.; Davidovich, P. B. DFT Quantum-Chemical Study of the Hydrolysis Products of Fe(II) and Fe(III) Aqua-Complexes. *Russ. J. Gen. Chem.* **2010**, *80*, 889−894.
(22) Aryanpour, M.; van Duin, A. C. T.; Kubicki, J. D. Development of a Reactive Force Field for Iron−Oxyhydroxide Systems. *J. Phys. Chem. A* **2010**, *114*, 6298−6307.
(23) Smith, W.; Leslie, M.; Forester, T. R. *The DL_Poly2 User Manual*, version 2.14; Daresbury Laboratory: Daresbury, Warrington, U.K., 2003.
(24) De Leeuw, N. H.; Cooper, T. G. Surface Simulation Studies of the Hydration of White Rust $Fe(OH)_2$, Goethite α-FeO(OH) and Hematite α-Fe_2O_3. *Geochim. Cosmochim. Acta* **2007**, *71*, 1655−1673.
(25) Dick, B. G.; Overhauser, A. W. Theory of the Dielectric Constants of Alkali Halide Crystals. *Phys. Rev.* **1958**, *112*, 90−103.
(26) De Leeuw, N. H.; Parker, S. C. Molecular-Dynamics Simulation of MgO Surfaces in Liquid Water using a Shell-Model Potential for Water. *Phys. Rev. B: Condens. Matter Mater. Phys.* **1998**, *58*, 13901−13908.
(27) Spagnoli, D.; Cooke, D. J.; Kerisit, S.; Parker, S. C. Molecular Dynamics Simulations of the Interaction between the Surfaces of Polar Solids and Aqueous Solutions. *J. Mater. Chem.* **2006**, *16*, 1997−2006.
(28) Duh, D.-M.; Perera, D. N.; Haymet, A. D. J. Structure and Properties of the CF1 Central Force Model of Water: Integral Equation Theory. *J. Chem. Phys.* **1995**, *102*, 3736−3746.
(29) Haymet, A. D. J. Dissociation and Solvation in Water and Aqueous Solutions. *J. Mol. Liq.* **1995**, *65*−*66*, 139−147.
(30) Stillinger, F. H.; Rahman, A. Revised Central Force Potentials for Water. *J. Chem. Phys.* **1978**, *68*, 666−670.
(31) Flynn, C. M. Hydrolysis of Inorganic Iron(III) Salts. *Chem. Rev.* **1984**, *84*, 31−41.
(32) Botti, A.; Bruni, F.; Imberti, S.; Ricci, M. A.; Soper, A. K. Ions in Water: The Microscopic Structure of Concentrated NaOH Solutions. *J. Chem. Phys.* **2004**, *120*, 10154−10162.
(33) Megyes, T.; Bálint, S.; Grósz, T.; Radnai, T.; Bakó, I.; Sipos, P. The Structure of Aqueous Sodium Hydroxide Solutions: A Combined Solution X-ray Diffraction and Simulation Study. *J. Chem. Phys.* **2008**, *128*, 044501.
(34) Magini, M.; Radnai, T. X-ray Diffraction Study of Ferric Chloride Solutions and Hydrated Melt. Analysis of the Iron (III)−Chloride Complexes Formation. *J. Chem. Phys.* **1979**, *71*, 4255−4262.
(35) Grant, M.; Jordan, R. B. Kinetics of Solvent Water Exchange on iron(III). *Inorg. Chem.* **1981**, *20*, 55−60.
(36) Swaddle, T. W.; Merbach, A. E. High-Pressure Oxygen-17 Fourier Transform Nuclear Magnetic Resonance Spectroscopy. Mechanism of Water Exchange on iron(III) in Acidic Aqueous Solution. *Inorg. Chem.* **1981**, *20*, 4212−4216.
(37) Hendrickson, W. A.; Co, M. S.; Smith, J. L.; Hodgson, K. O.; Klippenstein, G. L. X-Ray Absorption Spectroscopy of the Dimeric Iron Site in Azidomethemerythrin from Phascolopsis gouldii. *Proc. Natl. Acad. Sci. U. S. A.* **1982**, *79*, 6255−6259.
(38) Henry, M.; Jolivet, J. P.; Livage, J. In *Chemistry, Spectroscopy and Applications of Sol-Gel Glasses*; Reisfeld, P. R., JJørgensen, C. K., Eds.; Springer: Berlin, Heidelberg, 1992; pp 153−206.
(39) Brodholt, J. P. Molecular Dynamics Simulations of Aqueous NaCl Solutions at High Pressures and Temperatures. *Chem. Geol.* **1998**, *151*, 11−19.
(40) Michel, F. M.; Ehm, L.; Antao, S. M.; Lee, P. L.; Chupas, P. J.; Liu, G.; Strongin, D. R.; Schoonen, M. A. A.; Phillips, B. L.; Parise, J. B. The Structure of Ferrihydrite, a Nanocrystalline Material. *Science* **2007**, *316*, 1726−1729.
(41) Zhang, H.; Chen, B.; Ren, Y.; Waychunas, G. A.; Banfield, J. F. Response of Nanoparticle Structure to Different Types of Surface Environments: Wide-angle X-ray Scattering and Molecular Dynamics Simulations. *Phys. Rev. B: Condens. Matter Mater. Phys.* **2010**, *81*, 125444.
(42) Gebauer, D.; Völkel, A.; Cölfen, H. Stable Prenucleation Calcium Carbonate Clusters. *Science* **2008**, *322*, 1819−1822.
(43) Gebauer, D.; Cölfen, H. Prenucleation Clusters and Non-classical Nucleation. *Nano Today* **2011**, *6*, 564−584.
(44) Gebauer, D.; Kellermeier, M.; Gale, J. D.; Bergström, L.; Cölfen, H. Pre-Nucleation Clusters as Solute Precursors in Crystallisation. *Chem. Soc. Rev.* **2014**, *43*, 2348−2371.
(45) Baumgartner, J.; Dey, A.; Bomans, P. H. H.; Le Coadou, C.; Fratzl, P.; Sommerdijk, N. A. J. M.; Faivre, D. Nucleation and Growth of Magnetite from Solution. *Nat. Mater.* **2013**, *12*, 310−314.

DOI: 10.1021/acs.jpcb.5b03801
J. Phys. Chem. B 2015, 119, 10630−10642